Effects of Chromium Substitution on the Chemical Bonding Nature and Electrochemical Performance of Layered Lithium Manganese Oxide

Seong-Ju Hwang, Hyo-Suk Park, and Jin-Ho Choy*

National Nanohybrid Materials Laboratory, School of Chemistry and Molecular Engineering, Seoul National University, Seoul 151-747, Korea

Guy Campet

Institut de Chimie de la Matière Condensée de Bordeaux (ICMCB) du CNRS, Château Brivazac, Avenue du Dr. A. Schweitzer, 33608 Pessac, France

Received: April 27, 2000; In Final Form: May 23, 2000

Chromium-substituted $LiMn_{1-x}Cr_xO_2$ ($0 \le x \le 0.15$) oxides have been prepared by the ion-exchange reaction between α-$NaMn_{1-x}Cr_xO_2$ and LiBr. From the X-ray diffraction and infrared spectroscopic analyses, all of the present layered compounds are found to be crystallized with monoclinic structure. Additionally, the nitrogen adsorption−desorption isotherm measurements indicate a decrease in crystallite size induced by the replacement of Mn with Cr. According to the electrochemical measurements, the Cr-substituted compounds exhibit better electrochemical performance than the pristine $LiMnO_2$. The effects of chromium substitution on the chemical bonding nature of $LiMn_{1-x}Cr_xO_2$ have been investigated by performing X-ray absorption spectroscopic (XAS) analyses. The Cr K-edge XAS results presented here clarify that the trivalent chromium ions are stabilized in the octahedral site of the $(Mn,Cr)O_2$ layer before and after the electrochemical charge−discharge process. From the extended X-ray absorption fine structure analyses at the Mn K-edge, it becomes clear that the substitution of manganese with chromium gives rise to a shortening of the Mn−O bonds, leading to the stabilization of Mn in the octahedral site. On the basis of the present experimental findings, we suggest that the superior electrochemical performance of $LiMn_{1-x}Cr_xO_2$ can be attributed to the enhanced stability of the layered manganese oxide lattice because of the presence of a chromium ion in the octahedral site of the transition metal oxide layer, which hinders the migration of manganese ions into the interlayer lithium sites.

Introduction

The lithium transition metal oxides, $LiMO_2$ (M = Co, Ni, Mn, etc), have been extensively studied as an intercalation electrode in lithium secondary batteries, because they possess a unique two-dimensional crystal structure suitable for the fast conduction of interlayer lithium ions.[1,2] Among them, the layered $LiCoO_2$ compound has been successfully commercialized because of its high energy density and its excellent stability with respect to extended electrochemical cyclings.[3] However, from the economic and environmental points of view, the high cost and high toxicity of cobalt have led to considerable research efforts toward developing layered lithium manganate as an alternative cathode.[4,5] In contrast to the layered $LiCoO_2$ and $LiNiO_2$ compounds, layered $LiMnO_2$ cannot be synthesized using the conventional solid-state reaction, which is surely because of the similar size of Li^{I} and Mn^{III} ions and/or the presence of antiferromagnetic coupling between trivalent manganese ions.[6,7] Such a synthetic problem could be solved by applying the ion-exchange reaction between α-$NaMnO_2$ and LiBr (or LiCl) at low temperature.[8,9] According to electrochemical measurements, the layered $LiMnO_2$ compound exhibits a large initial capacity of more than 270 mAh/g but it suffers from severe capacity fading, which is surely ascribable to the irreversible transition to spinel-type structure.[8,10] Such a structural instability during the electrochemical charge−discharge cycle has also been observed for the spinel $LiMn_2O_4$ phase, giving rise to the suppression of charge capacity.[5] For this case, numerous attempts have been made to enhance the structural stability of this spinel oxide, which reveal that the partial substitution of manganese ions with other transition metal ions such as Cr^{III} and Co^{III} is quite effective in improving the cyclability of $LiMn_2O_4$ spinel.[11−14] Such a finding gives us the impetus to prepare the chromium-substituted $LiMn_{1-x}Cr_xO_2$ layered oxide. Recently, we found that this chromium-substituted phase has a better electrochemical performance than the unsubstituted $LiMnO_2$. Taking into account the fact that the electrochemical property of an intercalation compound is closely connected with its crystal and electronic structures, elucidating the effect of chromium substitution on the chemical bonding nature of layered $LiMnO_2$ is quite important in understanding the mechanism responsible for capacity fading as well as in designing new cathode materials. For this purpose, X-ray absorption spectroscopy (XAS) is expected to be very suitable, as this method allows us to probe in detail the local structure and electronic configuration of the absorbing metal ion, even for the poorly crystallized derivatives obtained after cycling. By virtue of such advantages, XAS has been successfully applied to the investigation of the intercalation mechanism of various cathode materials such as $LiMnO_2$, $LiMn_2O_4$, $LiNi_{1-x}Co_xO_2$, etc.[10,15−20]

In this work, we have prepared the chromium-substituted $LiMn_{1-x}Cr_xO_2$ layered oxides and characterized their physicochemical properties by using X-ray diffraction (XRD), infrared

* Author to whom correspondence should be addressed. Telephone: +82−2−880−6658. Fax: +82-2-872-9864. E-mail: jhchoy@plaza.snu.ac.kr.

10.1021/jp0016176 CCC: $19.00
Published on Web 07/25/2000

TABLE 1: Lattice Parameters, Crystal Symmetries, Unit Cell Volumes, and Chemical Formulas of the Layered $LiMn_{1-x}Cr_xO_2$ Compounds

sample	a (Å)	b (Å)	c (Å)	β (°)	V_c	chemical formula
$x = 0.00$	5.443	2.810	5.392	116.012	74.12	$Li_{1.02}MnO_2$
$x = 0.05$	5.441	2.809	5.394	116.023	74.08	$Li_{1.01}Mn_{0.94}Cr_{0.06}O_2$
$x = 0.10$	5.440	2.808	5.395	116.030	74.04	$Li_{1.01}Mn_{0.90}Cr_{0.11}O_2$
$x = 0.15$	5.439	2.807	5.395	116.023	74.02	$Li_{1.02}Mn_{0.84}Cr_{0.16}O_2$

spectroscopy (IR), N_2 adsorption−desorption isotherms, and electrochemical measurements. Also, Mn and Cr K-edge XAS analyses have been performed to study the effect of chromium substitution on the chemical bonding character of the layered lithium manganese oxides. In addition, we have examined the evolution of the local structure and electronic configuration of the chromium and manganese ions during the electrochemical lithium deintercalation−intercalation reaction, which should provide some clues for stabilizing the lithium manganate cathode during the electrochemical charge−discharge process.

Experimental Section

Sample Preparation. The polycrystalline $LiMn_{1-x}Cr_xO_2$ samples have been prepared by the ion-exchange reaction of α-$NaMn_{1-x}Cr_xO_2$ with LiBr. The precursor α-$NaMn_{1-x}Cr_xO_2$ was obtained by heating a mixture of Na_2CO_3, Mn_2O_3, and Cr_2O_3 (mole ratio = 1.1:1−x:x) at 725−745 °C for 40 h with intermittent grindings. The ion-exchange reaction was performed by reacting α-$NaMn_{1-x}Cr_xO_2$ with 10 equiv of lithium bromide in an *n*-hexanol solution at 148 °C for 48 h. The resulting precipitate was filtered, washed with *n*-hexanol and methanol, and dried in a vacuum. In contrast to the very hygroscopic nature of the unsubstituted α-$NaMnO_2$ precursor, the Cr-substituted compounds were found to be rather stable in an ambient atmosphere.

Sample Characterization. The crystal structures of the $LiMn_{1-x}Cr_xO_2$ samples were studied by XRD measurements using Ni-filtered Cu Kα radiation with a graphite diffracted beam monochromator, and their chemical compositions were determined by performing atomic absorption (AA) spectrometry. As listed in Table 1, the present AA results indicate that the chromium ion is successfully incorporated into the crystal lattice of layered lithium manganate. The IR spectra in the frequency range of 300−800 cm^{-1} were recorded on a BOMEM MB-102 Fourier transform spectrometer. Prior to the measurements, the samples were finely pulverized, mixed with KBr, and pressed into translucent pellets. To determine the surface area and porosity of layered lithium manganates, the nitrogen adsorption−desorption isotherms were measured volumetrically at the liquid nitrogen temperature with a homemade computer-controlled measurement system. The calcined samples were degassed at 300 °C for 3 h under vacuum prior to the adsorption measurement. The electrochemical measurements were performed with the cell of Li/1M $LiPF_6$ in EC:DEC (50:50 v/v)/$LiMn_{1-x}Cr_xO_2$, which was assembled in a drybox. The composite cathode was prepared by thoroughly mixing the active $LiMn_{1-x}Cr_xO_2$ cathode material (85%) with 10% of acetylene black and 5% of PTFE [poly(tetrafluoroethylene)]. All of the experiments were carried out in the galvanostatic mode with an Arbin BT 2043 multichannel galvanostat/potentiostat in the voltage range of 2.2−4.3 V.

X-ray Absorption Measurements. The XAS experiments were performed for $LiMn_{1-x}Cr_xO_2$ ($x = 0$, 0.05, 0.10, and 0.15) and their cycled derivatives by using the extended X-ray absorption fine structure (EXAFS) facility installed at beam line 7C at the Photon Factory in Tsukuba, Japan.[21] After the first charge−discharge cycle, the samples were mounted on the sample holder with Kapton window tape in an Ar-filled drybox, in order to protect against humidity. The XAS data were collected at room temperature in transmission mode using gas-ionization detectors. All of the present spectra were calibrated by measuring the spectra of Cr and Mn metal foils. The data analysis for the experimental spectra was performed by the standard procedure, as reported previously.[10,15] All of the present X-ray absorption near-edge structure (XANES) spectra were normalized by fitting the smooth EXAFS high-energy region with a linear function after subtracting the background extrapolated from the pre-edge region. The EXAFS oscillations were separated from the absorption background by using a cubic spline background-removal technique. The resulting $\chi(k)$ oscillations were weighted with k^3 in order to compensate for the diminishing amplitude of the EXAFS at the high k region. For analyzing the EXAFS data, nonlinear least-squares curve fitting was carried out for the Fourier-filtered coordination shells by minimizing the value of F $\{F = [\sum k^6(\chi_{cal} - \chi_{exp})^2]^{1/2}/n$, where the summation was performed over the data points (n) in the analyzed k range} with the use of the well-known single-scattering EXAFS theory.[22]

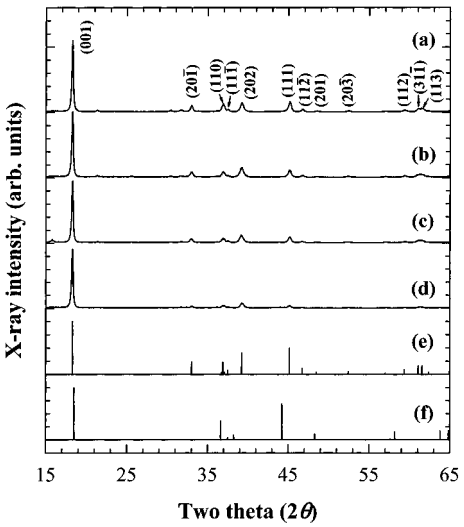

Figure 1. Powder XRD patterns for the layered $LiMn_{1-x}Cr_xO_2$ compounds with x = (a) 0, (b) 0.05, (c) 0.10, and (d) 0.15, in comparison with the simulated data for layered $LiMnO_2$ phase with (e) monoclinic and (f) rhombohedral structures.

Results and Discussion

Powder XRD Analysis. The powder XRD patterns of the pristine $LiMn_{1-x}Cr_xO_2$ ($x = 0$, 0.05, 0.10, and 0.15) compounds are shown in Figure 1, together with the simulated data for the layered $LiMnO_2$ phases with monoclinic and rhombohedral symmetries. Except for some small reflections at low angle corresponding to the impurity Li_2MnO_3 and orthorhombic $LiMnO_2$ phases, all of the intense XRD peaks of $LiMn_{1-x}Cr_xO_2$ can be well indexed on the basis of the α-$NaFeO_2$-type layered structure with a monoclinic distortion. Although the recent study on layered $LiMn_{1-x}Co_xO_2$ oxides reported that the partial substitution of manganese with cobalt induces a structural modification from monoclinic to rhombohedral,[23] the theoretical simulation results clarify that the present data for $LiMn_{1-x}Cr_xO_2$ are not consistent with the rhombohedral structure. The lattice parameters and unit cell volumes were calculated from least-squares fitting analysis, as listed in Table 1. Whereas the in-plane lattice parameters decrease with increasing Cr substitution rate, the basal spacings expand on replacement of manganese

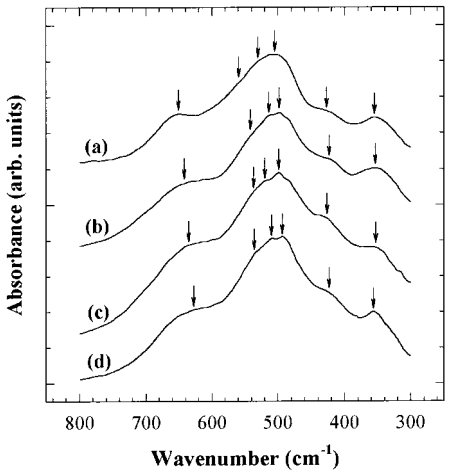

Figure 2. Infrared spectra for the layered $LiMn_{1-x}Cr_xO_2$ compounds with x = (a) 0, (b) 0.05, (c) 0.10, and (d) 0.15.

with chromium. Such a contrasted evolution of lattice parameters can be understood as a result of the substitution of Mn with Cr, leading to the differences in the variation of the average $M-O_{eq}$ and $M-O_{ax}$ bond distances, which will be discussed in detail in the following EXAFS section. As summarized in Table 1, the unit cell volumes of the pristine lithium manganates are found to decrease as the chromium substitution rate increases, suggesting that the Mn^{III} ion is surely replaced by the relatively smaller Cr^{III} ion [$Mn^{III}(6) = 0.65$ Å, $Cr^{III}(6) = 0.62$ Å, where the number in parentheses represents the coordination number[6]].

IR Spectroscopic Analysis. The IR spectra of the pristine $LiMn_{1-x}Cr_xO_2$ (x = 0, 0.05, 0.10, and 0.15) compounds are presented in Figure 2. According to the group theoretical calculation, the layered lithium metal oxide with monoclinic $C2/m$ symmetry is predicted to show six infrared-active $2B_u + 2A_u + 2B_u$ modes, whereas there are four infrared-active $2A_u + 2E_u$ modes for the rhombohedral $R-3m$ phase.[24] In the case of the present $LiMnO_2$ compound, six IR bands are discernible in the frequency range 300−800 cm^{-1}, pointing to the monoclinic symmetry of this compound. As shown in Figure 2, all of the present compounds exhibit nearly the same spectral characteristics, implying that the monoclinic layered structure is maintained for the substitution range of $0 \le x \le 0.15$, which is fully consistent with the XRD results. Such a finding is further supported by the recent Raman results indicating that three phonon lines corresponding to monoclinic $C2/m$ symmetry are observed for $LiMn_{1-x}Cr_xO_2$ compounds; these results will be published elsewhere.

N_2 Adsorption−Desorption Analysis. The N_2 adsorption−desorption isotherms for $LiMn_{1-x}Cr_xO_2$ (x = 0, 0.05, 0.10, and 0.15) are plotted in Figure 3. From theoretical calculation based on the BET formula, the surface area is determined to be 16 m^2/g for x = 0, 25 m^2/g for x = 0.05, 42 m^2/g for x = 0.10, and 59 m^2/g for x = 0.15, indicating an increase in surface area caused by the substitution of Mn with Cr. No hysteresis of the N_2 adsorption−desorption isotherm could be detected for the range $p/p_0 \le 0.8$, suggesting that there are no meso- or micropores in the present samples.[25] Therefore, most of the nitrogen adsorption−desorption activity is considered to occur on the sample surface. In this respect, the enhancement of the surface area upon Cr substitution can be interpreted as a result of the decrease in crystallite size rather than an increase in porosity,[26] which implies that the partially substituted chromium ion hinders the crystal growth of lithium manganese oxide.

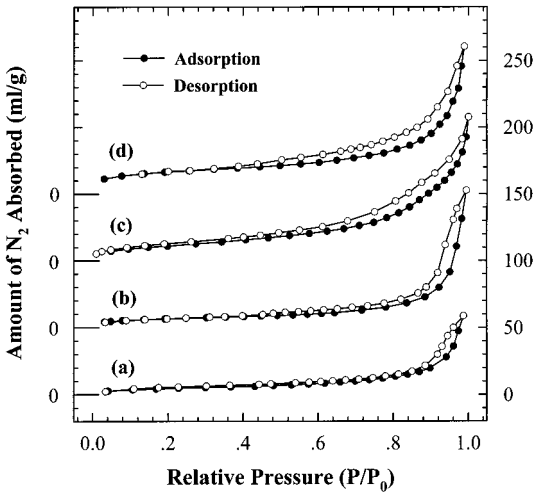

Figure 3. N_2 adsorption−desorption isotherms for the layered $LiMn_{1-x}Cr_xO_2$ compounds with x = (a) 0, (b) 0.05, (c) 0.10, and (d) 0.15.

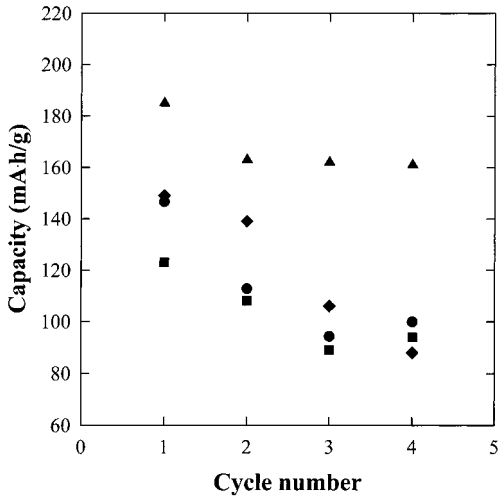

Figure 4. Discharge capacities of the layered $LiMn_{1-x}Cr_xO_2$ compounds with x = 0 (squares), 0.05 (circles), 0.10 (triangles), and 0.15 (diamonds). The electrochemical measurements were carried out in the potential range of 2.2−4.3 V with an applied current density of 0.5 mA/cm^2.

Electrochemical Performance. Figure 4 presents the variation of the discharge capacity of $LiMn_{1-x}Cr_xO_2$ (x = 0, 0.05, 0.10, and 0.15) with respect to the cycle number. The substitution of Mn with Cr improves the electrochemical performance of unsubstituted $LiMnO_2$ and depresses severe capacity fading after the first charging process, as observed for the cobalt-substituted $LiMn_{1-x}Co_xO_2$ phase.[23] Among the present materials, the $LiMn_{0.9}Cr_{0.1}O_2$ compound with the 10% Cr substitution rate exhibits the best electrochemical property. In the case of an applied current density of 0.5 mA/cm^2, this compound retains a prominent capacity of >150 mAh/g after four electrochemical cycles, which is much greater than the corresponding value for the unsubstituted $LiMnO_2$ compound (~100 mAh/g). When we decrease the current density to 0.2 mA/cm^2, $LiMn_{0.9}Cr_{0.1}O_2$ shows a capacity of more than 200 mAh/g, which is greater than that of unsubstituted $LiMnO_2$ (170 mAh/g). Detailed studies on the long-term cycling characteristics of $LiMn_{1-x}Cr_xO_2$ are presently underway for various current densities, to clarify the relationship between electrochemical performance and Cr substitution in the layered lithium manganate cathode. The capacity−potential profile of $LiMn_{0.9}Cr_{0.1}O_2$ is depicted in

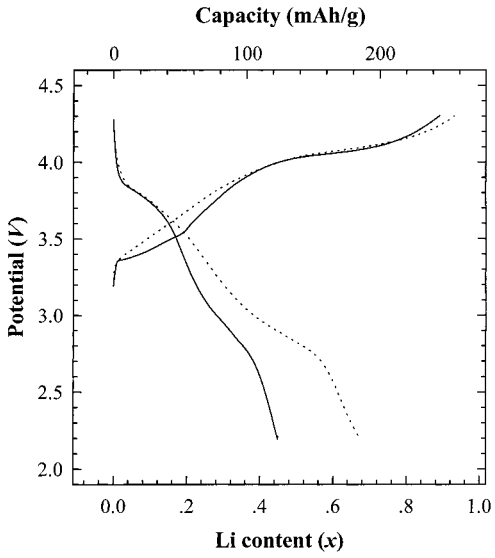

Figure 5. First charge−discharge profiles of the layered $LiMn_{1-x}Cr_xO_2$ compounds with $x = 0$ (solid lines) and 0.1 (dotted lines). The electrochemical measurements were carried out in the potential range of 2.2−4.3 V with an applied current density of 0.5 mA/cm^2.

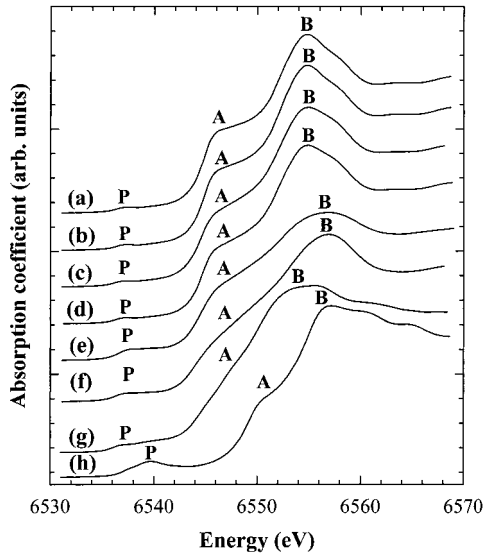

Figure 6. Mn K-edge XANES spectra for the layered $LiMn_{1-x}Cr_xO_2$ compounds with $x =$ (a) 0, (b) 0.05, (c) 0.10, and (d) 0.15, and the electrochemically cycled $LiMn_{1-x}Cr_xO_2$ with $x =$ (e) 0 and (f) 0.10, in comparison with those for the references (g) Mn_2O_3 and (h) MnO_2.

Figure 5, in comparison with that of $LiMnO_2$. In the first charge−discharge curve, the layered $LiMnO_2$ shows two pseudo-plateaus near 3 and 4 V, which demonstrates the partial formation of a spinel-like domain induced by lithium deintercalation. Such formation of plateaus is less prominent for the chromium-substituted sample than for the unsubstituted sample, clarifying that the substitution of Mn with Cr suppresses the structural transition from the layered structure to the spinel structure.

Mn K-Edge XANES Analysis. To elucidate the origin of the stabilization of the layered structure upon chromium substitution, the chemical bonding character of layered lithium chromium manganates has been investigated using XANES spectroscopy. The Mn K-edge XANES spectra for $LiMn_{1-x}Cr_xO_2$ ($x = 0$, 0.05, 0.10, and 0.15) are shown in Figure 6, in comparison with reference spectra for Mn_2O_3 and MnO_2. Regardless of the chromium substitution rate, all of the lithium chromium manganates exhibit common spectral features that are characteristic of the layered $LiMnO_2$ phase, indicative of the same chemical environment of manganese ion in the present compounds. In the pre-edge region, a small peak P, corresponding to the quadrupole-allowed 1s → 3d transition, is observed in all of the spectra presented here.[10] Because the intensity of this peak is proportional to the distortion of local structure around the absorbing metal ion from inversion symmetry,[27] the negligible intensity of this peak implies that all of the manganese ions in the samples under investigation are stabilized in the octahedral site with an inversion center. In addition, the position of this pre-edge peak for $LiMn_{1-x}Cr_xO_2$ is found to be nearly the same as that for the reference Mn_2O_3, indicating the trivalent oxidation state of manganese ion. In the main-edge region, there are two strong peaks corresponding to the dipole-allowed transitions from the core 1s level to the unoccupied 4p level. On the basis of the previously reported simulation results,[10] the presence of the strong peak A for $LiMn_{1-x}Cr_xO_2$ can be regarded as clear evidence for the presence of trivalent manganese ion stabilized in the tetragonally distorted octahedra over the present Cr-substitution range ($0 \le x \le 0.15$). As the chromium substitution rate increases, the main-edge features A and B become rather broader, reflecting the increase in disorder in the local environment around manganese. Such a finding is contrasted by the previous results for Cr-substituted $LiMn_{2-x}Cr_xO_4$ spinel, which showed that the chromium substitution eliminates the local disorder near the MnO_6 octahedra by reducing the concentration of the Jahn−Teller active Mn^{III} ion.[18] In the present layered $LiMn_{1-x}Cr_xO_2$ compounds, chromium substitution does not modify the oxidation state of manganese but increases the local disorder around manganese through the replacement of neighboring manganese ions with chromium ions.

On the basis of the above XANES results, the evolution of the chemical environment around manganese upon electrochemical cycling has also been examined by performing ex situ XANES analyses for $LiMn_{1-x}Cr_xO_2$ ($x = 0$ and 0.10). As shown in Figure 6, the electrochemical charge−discharge process gives rise to a blue shift of the edge position, suggesting an increase in the Mn oxidation state because of the irreversibility of lithium deintercalation/intercalation.[8] This is further evidenced by the displacement of the pre-edge peak P toward the high energy side. Significant changes in the overall spectral features are also observed for both electrochemically cycled samples, confirming that the layered structure is irreversibly altered by the electrochemical delithiation process. However, it is worthwhile to note here that the suppression of spectral features A and B is less pronounced for the Cr-substituted compound than for the unsubstituted compound, indicating that the chromium substitution hinders the structural transition induced by electrochemical cycling.

Cr K-Edge XANES Analysis. Figure 7 illustrates the Cr K-edge XANES spectra for $LiMn_{1-x}Cr_xO_2$ ($x = 0.05$, 0.10, and 0.15) and the reference spectra for Cr_2O_3 and CrO_3. The edge energies of lithium chromium manganese oxides are almost identical to those of Cr_2O_3, suggesting the trivalent oxidation state of chromium in these compounds. Whereas the pre-edge peak P related to the quadrupole-allowed 1s → 3d transition is fairly weak in intensity for $LiMn_{1-x}Cr_xO_2$ and Cr_2O_3 with trivalent chromium ion in the octahedral site, a very intense feature P is detected for the reference CrO_3 with the tetrahedral Cr^{VI} ion. Such an inconsistency is attributed to the difference not only in the hole concentrations of Cr 3d orbitals but also in the local symmetry around chromium, i.e., O_h for the former

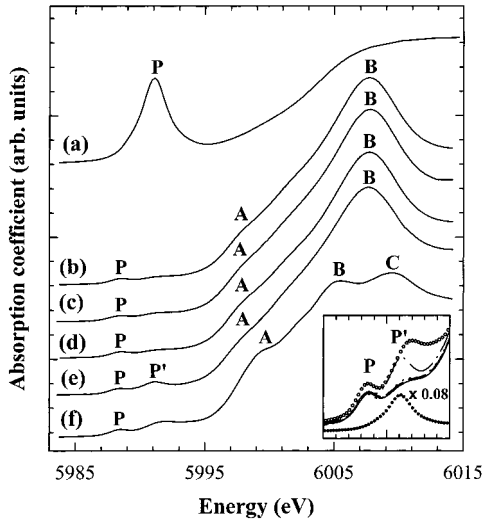

Figure 7. Cr K-edge XANES spectra for the layered $LiMn_{1-x}Cr_xO_2$ compounds with $x =$ (b) 0.05 (solid lines), (c) 0.10 (dotted lines), and (d) 0.15 (dashed lines), (e) the electrochemically cycled $LiMn_{0.90}Cr_{0.10}O_2$ (dot-dashed circles), in comparison with those for the references (a) CrO_3 (solid circles) and (f) Cr_2O_3 (open circles). The inset provides enlarged views of all the present spectra with an energy range of 5985−5995 eV. The information in parentheses is for the curves in the inset.

and T_d for the latter. In this regard, the weak intensity of the pre-edge peak P for $LiMn_{1-x}Cr_xO_2$ allows us to exclude the possibility of a hexavalent chromium ion. As can be seen clearly from the inset of Figure 7, the pre-edge peak positions of the lithium chromium manganese oxides are similar to those of reference Cr_2O_3, confirming the presence of trivalent chromium ion in the layer lattice. In the main-edge region, the overall spectral features of all of the lithium chromium manganese oxides are nearly identical to one another, which supports the XRD results showing that all of the chromium ions are found to be successfully substituted into the octahedral site of the $(Mn,Cr)O_2$ layer.

On the other hand, the effect of electrochemical cycling on the chemical bonding character of chromium has also been investigated by performing ex situ XANES analysis. Except for the appearance of the small additional pre-edge peak (P′),[28] the overall spectral features of the pristine $LiMn_{0.90}Cr_{0.10}O_2$ compound remain unchanged before and after the electrochemical charge−discharge process, indicating negligible change in the electronic structure and symmetry of the chromium ion. On the basis of the above experimental findings, it can be suggested that the local chemical environment of chromium is not significantly perturbed by the electrochemical delithiation/relithiation process.

Mn K-Edge EXAFS Analysis. The local structure of manganese ion in the layered $LiMn_{1-x}Cr_xO_2$ compounds has been quantitatively determined by using EXAFS spectroscopy. The k^3-weighted Mn K-edge EXAFS spectra for $LiMn_{1-x}Cr_xO_2$ ($x =$ 0, 0.05, 0.10, and 0.15) are Fourier transformed in the k range of 3.8−12.55 $Å^{-1}$, as shown in Figure 8a. All of the layered lithium manganates exhibit three intense Fourier transform (FT) peaks at ∼1.6, ∼2.2, and ∼2.7 Å, which are attributed to the Mn−O, Mn−M, and Mn−M shells (M = Mn or Cr), respectively. Because the splitting of the Mn−M shells originates from the Jahn−Teller distortion of trivalent manganese ion, the observation of three FT peaks for the Cr-substituted phases certifies that the monoclinic symmetry of layered lithium manganate is not significantly modified by replacing manganese with chromium, in complete agreement with the XRD results.

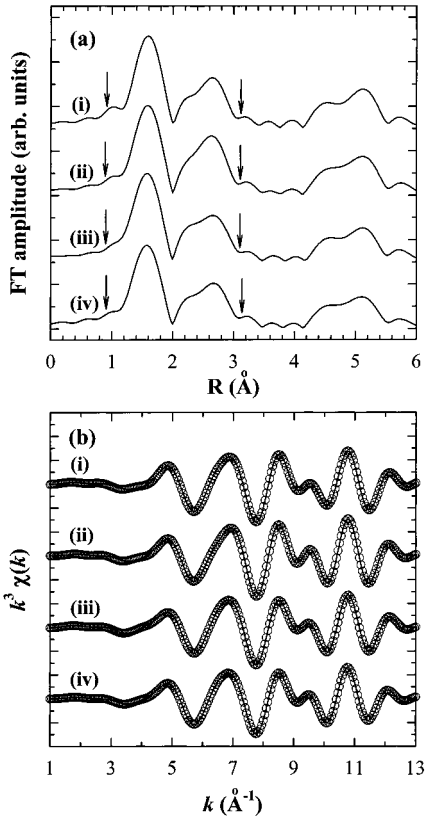

Figure 8. (a) Fourier transformed Mn K-edge EXAFS spectra and (b) the inverse Fourier transforms for the layered $LiMn_{1-x}Cr_xO_2$ compounds with $x =$ (i) 0, (ii) 0.05, (iii) 0.10, and (iv) 0.15. The range over which Fourier filtering has been applied is shown by the arrows. The solid lines and empty circles represent the fitted and experimental data, respectively.

TABLE 2: Results of Nonlinear Least-Squares Curve-Fitting Analysis for the Mn K-edge EXAFS Spectra of the Layered $LiMn_{1-x}Cr_xO_2$ Compounds

sample	bond	*CN*	*R* (Å)	σ^2 (10^{-3} Å^2)
$LiMnO_2$	Mn−O_{eq}	4	1.91	1.69
	Mn−O_{ax}	2	2.32	3.32
	Mn−M	2	2.80	3.00
	Mn−M	4	3.04	6.12
$LiMn_{0.95}Cr_{0.05}O_2$	Mn−O_{eq}	4	1.90	2.20
	Mn−O_{ax}	2	2.30	4.15
	Mn−M	2	2.79	2.68
	Mn−M	4	3.04	6.06
$LiMn_{0.90}Cr_{0.10}O_2$	Mn−O_{eq}	4	1.90	2.63
	Mn−O_{ax}	2	2.29	6.02
	Mn−M	2	2.80	3.10
	Mn−M	4	3.04	7.46
$LiMn_{0.85}Cr_{0.15}O_2$	Mn−O_{eq}	4	1.90	2.93
	Mn−O_{ax}	2	2.29	4.67
	Mn−M	2	2.80	3.17
	Mn−M	4	3.04	7.18

To perform the nonlinear curve fitting analysis, the FT spectra were inversely Fourier transformed to k space (Figure 8b). All of the present compounds show nearly the same EXAFS oscillation, which can be well reproduced on the basis of α-$NaMnO_2$-type layered structure with a monoclinic distortion.[29] The best-fit results are compared to the experimental spectra in Figure 8b, and the best-fit structural parameters are summarized in Table 2. The manganese ion in the layered $LiMn_{1-x}Cr_xO_2$ is revealed to be stabilized in a tetragonally distorted octahedron, confirming the existence of Jahn−Teller distortion around the manganese ion. It is also determined from the curve-fitting

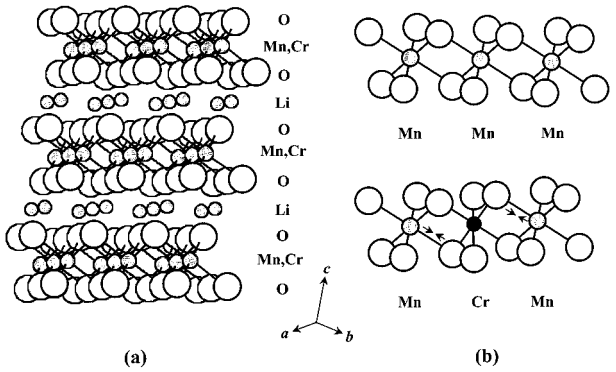

Figure 9. (a) Crystal structure for chromium-substituted $LiMn_{1-x}Cr_xO_2$ layered oxide and (b) schematic model for evolution of local structure around manganese induced by chromium substitution.

TABLE 3: Results of Nonlinear Least-Squares Curve-Fitting Analysis for the Cr K-edge EXAFS Spectra of the Layered $LiMn_{1-x}Cr_xO_2$ Compounds and the Electrochemically Cycled $LiMn_{0.9}Cr_{0.1}O_2$

sample	bond	*CN*	*R* (Å)	σ^2 (10^{-3} Å^2)
$LiMn_{0.95}Cr_{0.05}O_2$	Cr−O	6	1.97	4.26
	Cr−M	6	2.91	8.99
$LiMn_{0.90}Cr_{0.10}O_2$	Cr−O	6	1.97	4.00
	Cr−M	6	2.91	7.75
$LiMn_{0.85}Cr_{0.15}O_2$	Cr−O	6	1.97	4.19
	Cr−M	6	2.91	8.58
cycled $LiMn_{0.9}Cr_{0.1}O_2$	Cr−O	6	1.97	3.00
	Cr−M	6	2.91	9.81

analysis that both the $Mn-O_{eq}$ and the $Mn-O_{ax}$ bonds are commonly shortened as the chromium content increases, which is in good agreement with the contraction of the cell volume upon Cr substitution. In addition, the decrease in the axial Mn−O bond distance appears to be more prominent than that in the equatorial distance. For a clear understanding of this dissimilar evolution of both manganese−oxygen bonds, the effect of Cr substitution on the local structure around manganese is illustrated in Figure 9. In the case where the longer $Mn-O_{ax}$ bond is parallel to the shorter $Cr-O_{ax}$ bond, the former would be shortened because of the geometric strain originating from the remarkable distance difference between the two bonds (Tables 2 and 3). In contrast, the equatorial Mn−O bond is less influenced upon chromium substitution, because the bond lengths are rather similar for both $Mn-O_{eq}$ and $Cr-O_{eq}$. Consequently, the structural distortion due to the Jahn−Teller effect is relieved by Cr substitution. As shown in Table 2, the Debye−Waller factor is enhanced by increasing the chromium concentration, verifying the existence of a remarkable increase in structural disorder upon chromium substitution. This finding is well correlated with the broadening of XANES features A and B for the Cr-substituted phases.

Cr K-Edge EXAFS Analysis. The FTs of k^3-weighted Cr K-edge EXAFS spectra for $LiMn_{1-x}Cr_xO_2$ ($x = 0.05$, 0.10, and 0.15) are plotted in Figure 10a, and the corresponding Fourier-filtered oscillations in Figure 10b. There are close similarities in the three spectra of the lithium chromium manganese oxides, which confirms that the chromium ion is present in the same crystal position over the present substitution range ($0 < x \leq 0.15$). In contrast to the Mn K-edge data in which three FT peaks appear, only two FT features are observed at around 1.5 and 2.5 Å in the Cr K-edge spectra, which correspond to the Cr−O and Cr−M shells (M = Mn or Cr), respectively. This confirms that the substituted chromium ion is placed in a regular octahedron, which is attributed to the absence of Jahn−Teller

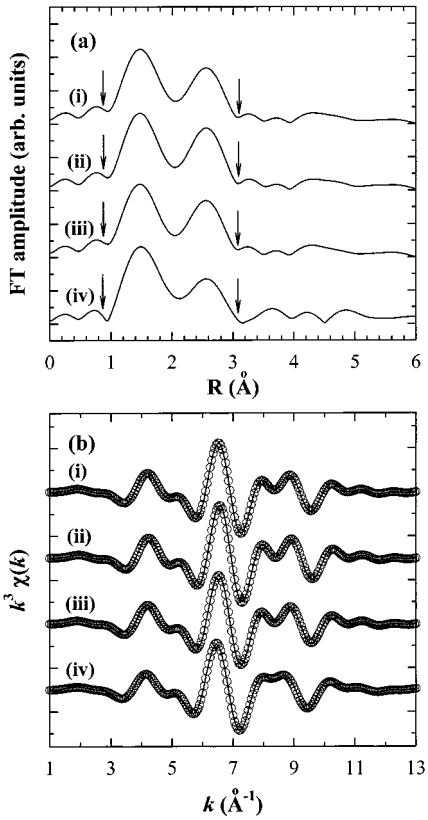

Figure 10. (a) Fourier transformed Cr K-edge EXAFS spectra and (b) the inverse Fourier transforms for the layered $LiMn_{1-x}Cr_xO_2$ compounds with $x =$ (i) 0.05, (ii) 0.10, and (iii) 0.15, and (iv) for cycled $LiMn_{0.9}Cr_{0.1}O_2$. The range over which Fourier filtering has been applied is shown by the arrows. The solid lines and empty circles represent the fitted and experimental data, respectively.

distortion in the trivalent chromium ion with an electronic configuration of [Ar]$3d^3$. In this respect, we have attempted to fit these spectra on the basis of a regular CrO_6 octahedron with six equally separated neighboring metal ions, in such a way that we were able to obtain reasonable fitting results. The best-fit results are compared to the experimental spectra in Figure 10a, and the best-fit structural parameters are listed in Table 3. As expected, the chromium ion is found to be stabilized in the regular octahedron with a Cr−O bond distance of 1.97 Å, which is consistent with the bond length of $Cr^{III}-O$ in Cr-substituted spinel $LiMn_{2-x}Cr_xO_4$ (1.98 Å).[18] For these compounds, there are only negligible discrepancies in bond distances and Debye−Waller factors, suggesting that the chemical environment of the chromium ion is nearly independent of the chromium substitution rate. Comparing the determined Cr−O bond distances with those of Mn−O, the axial metal−oxygen bond is shorter for the former than for the latter, whereas the equatorial Cr−O bond distance is greater than the corresponding Mn−O distance. In this respect, the increase in the *c*-axis lattice parameter upon substitution of Mn with Cr can be understood as a result of the replacement of the shorter $Mn-O_{eq}$ bond with the longer $Cr-O_{eq}$ bond, because the basal spacing is mainly dependent on the equatorial metal−oxygen bond distance (Figure 9).

In addition, the evolution of the local structure around chromium upon electrochemical cycling has been quantitatively determined by performing ex situ EXAFS analyses at the Cr K-edge. As shown in Figure 10, the FT and inverse FT data for the cycled $LiMn_{0.9}Cr_{0.1}O_2$ compound are nearly identical to those for the pristine compound. In this respect, these data can be well reproduced with the same local structure of the chro-

mium ion, that is, a CrO_6 regular octahedron with six neighboring metal ions at the same distance. As listed in Table 3, the bond distances and Debye−Waller factors are almost the same for the pristine and cycled $LiMn_{0.9}Cr_{0.1}O_2$ compounds, which highlights the fact that most of the trivalent chromium ions are fixed in the octahedral sites of the $(Mn,Cr)O_2$ layer before and after the electrochemical charge−discharge process.

Stabilization of Layered Structure upon Chromium Substitution. From the present Mn K-edge EXAFS analyses, it becomes clear that the substitution of manganese with chromium gives rise to a shortening of the Mn−O bonds, leading to the stabilization of Mn in octahedral sites. Previously, we suggested that the manganese ion in the MnO_2 block of $LiMnO_2$ moves into the octahedral lithium site in the interlayer space preferentially along the line of $O_h \rightarrow T_d \rightarrow O_h \rightarrow T_d \rightarrow O_h$.[10] In this regard, the more prominent shrinkage of the axial Mn−O bond with respect to the corresponding equatorial bond is considered to play an important role in blocking the migration pathway of manganese from O_h to adjacent T_d and vice versa.[30] On the other hand, the Cr K-edge XAS results highlight the fact that the trivalent chromium ion is fixed to the octahedral site in the $(Mn,Cr)O_2$ layer before and after electrochemical cycling, which is surely ascribed to the large octahedral stabilization energy of trivalent chromium ion with the d^3 configuration. Such a fixation of chromium would also hinder the migration of manganese ions, as the displacement of metal ions promotes the migration of adjacent metal ions by reducing the potential barrier for conduction. On the basis of the present experimental findings, it can be concluded that the enhanced cyclability of Cr-substituted $LiMn_{1-x}Cr_xO_2$ compounds should be ascribed to the suppression of the transition to the spinel structure upon electrochemical cycling. Additionally, it is also suggested that the decrease in the monoclinic distortion upon Cr substitution contributes partially to the excellent electrochemical performance of $LiMn_{1-x}Cr_xO_2$ compounds.[23]

Conclusion

We were able to prepare chromium-substituted $LiMn_{1-x}Cr_xO_2$ ($0 \le x \le 0.15$) oxides and to characterize those compounds with X-ray diffraction, infrared spectroscopy, and nitrogen adsorption−desorption isotherm measurements. The electrochemical studies demonstrate that the substitution of Mn with Cr gives rise to an improvement in electrochemical performance. According to the XANES/EXAFS results presented here, it is certain that the trivalent chromium ion is fixed to the octahedral site in the $(Mn,Cr)O_2$ layer before and after electrochemical cycling, and the local structural variation of manganese in $LiMn_{1-x}Cr_xO_2$ upon lithium deintercalation/intercalation is suppressed by the substitution of manganese with chromium. On the basis of the present experimental findings, the superior electrochemical performance of $LiMn_{1-x}Cr_xO_2$ is surely due to an enhanced stability of the layered manganese oxide lattice caused by the presence of chromium ions in octahedral sites of the transition metal oxide layer, which hinders the migration of manganese ions into the interlayer lithium sites.

Acknowledgment. This work was supported in part by the Ministry of Science & Technology through the 1999 National Research Laboratory (NRL) project. The authors are grateful to Prof. M. Nomura for helping us obtain the XAS data in the Photon Factory, as well as to Dr. Y. S. Hong and Mr. C. W. Kwon for helping us measure the electrochemical performance. H. S. Park thanks to the Ministry of Education for the Brain Korea 21 fellowship.

References and Notes

(1) Mizushima, K.; Jones, P. C.; Wiseman, P. J.; Goodenough, J. B. *Mater. Res. Bull.* **1980**, *15*, 783.

(2) Dahn, J. R.; von Sacken, U.; Jukow, M. R.; Al-Janaby, H. *J. Electrochem. Soc.* **1991**, *138*, 2207.

(3) Nagaura, T.; Tazawa, K. *Prog. Batteries Sol. Cells* **1990**, *9*, 20.

(4) Thackeray, M. M.; Johnson, P. J.; de Piccioto, L. A.; Bruce, P. G.; Goodenough, J. B. *Mater. Res. Bull.* **1984**, *19*, 179.

(5) Thackeray, M. M. *Prog. Solid State Chem.* **1997**, *25*, 1.

(6) Shannon, R. D. *Acta Crystallogr. A* **1976**, *32*, 751.

(7) Ceder, G.; Mishra, S. K. *Electrochem. Solid-State Lett.* **1999**, *2*, 550.

(8) Armstrong, A. R.; Bruce, P. G. *Nature* **1996**, *381*, 499.

(9) Capitaine, F.; Gravereau, P.; Delmas, C. *Solid State Ionics* **1996**, *89*, 197.

(10) Hwang, S. J.; Park, H. S.; Choy, J. H.; Campet, G. *Chem. Mater.*, in press.

(11) Guohua, L.; Ikuta, H.; Uchida, T.; Wakihara, M. *J. Electrochem. Soc.* **1996**, *143*, 178.

(12) Pistoia, G.; Antonini, A.; Rosati, R.; Bellitto, C.; Ingo, G. M. *Chem. Mater.* **1997**, *9*, 1443.

(13) Robertson, A. D.; Lu, S. H.; Averill, W. F.; Howard, W. F., Jr. *J. Electrochem. Soc.* **1997**, *144*, 3500.

(14) Sigala, C.; Verbaere, A.; Mansot, J. L.; Guyomard, D.; Piffard, Y.; Tournoux, M. *J. Solid State Chem.* **1997**, *132*, 372.

(15) Treuil, N.; Labrugère, C.; Menetrier, M.; Portier, J.; Campet, G.; Deshayes, A.; Frison, J. C.; Hwang, S. J.; Song, S. W.; Choy, J. H. *J. Phys. Chem. B* **1999**, *103*, 2100.

(16) Choy, J. H.; Kim, D. H.; Kwon, C. W.; Hwang, S. J.; Kim, Y. I. *J. Power Sources* **1999**, *77*, 1.

(17) Chang, S. H.; Kang, S. G.; Song, S. W.; Yoon, J. B.; Choy, J. H. *Solid State Ionics* **1996**, *86−88*, 171.

(18) Ammundsen, B.; Jones, D. J.; Rozière, J.; Villain, F. *J. Phys. Chem. B* **1998**, *102*, 7939.

(19) Hong, S. J.; Chang, S. H.; Yo, C. H. *Bull. Korean Chem. Soc.* **1999**, *20*, 53.

(20) Shiraishi, Y.; Nakai, I.; Tsubata, T.; Himeda, T.; Nishikawa, F. *J. Solid State Chem.* **1997**, *133*, 587.

(21) Oyanagi, H.; Matsushida, T.; Ito, M.; Kuroda, H. *KEK Rep.* **1984**, *83*, 30.

(22) Teo, B. K. *EXAFS: Basic Principles and Data Analysis*; Springer-Verlag: Berlin, 1986.

(23) Armstrong, A. R.; Gitzendanner, R.; Robertson, A. D.; Bruce, P. G. *Chem. Commun.* **1998**, 1833.

(24) Inaba, M.; Iriyama, Y.; Ogumi, Z.; Todzuka, Y.; Tasaka, A. *J. Raman Spectrosc.* **1997**, *28*, 613.

(25) Choy, J. H.; Park, J. H.; Yoon, J. B. *J. Phys. Chem. B* **1998**, *102*, 5991.

(26) Assuming that the crystallite is cubic in shape, the particle size was calculated to be 90 nm for $x = 0$, 55 nm for $x = 0.05$, 34 nm for $x = 0.10$, and 25 nm for $x = 0.15$.

(27) Hahn, J. E.; Scott, R. A.; Hodgson, K. O.; Doniach, S.; Desjardins, S. R.; Solomon, E. I. *Chem. Phys. Lett.* **1982**, *88*, 595.

(28) The observation of pre-edge peak P′ indicates the partial formation of hexavalent chromium ion by charging at 4.3 V. In fact, the electrochemical study on the chromium-substituted $LiMn_{2-x}Cr_xO_4$ spinel oxide reveals that the oxidation of Cr^{III} to Cr^{VI} occurs in the potential range of 4.3−5.1 V (ref 14). In this respect, such formation of the Cr^{VI} species would be ruled out by decreasing the charging potential.

(29) The EXAFS oscillation of cycled $LiMn_{0.9}Cr_{0.1}O_2$ derivative (not shown) is found to be quite different from that of the pristine compound. In this regard, we cannot obtain reasonable fitting results with the α-$NaMnO_2$-type layered structure, which confirms the remarkable modification of the local structure of Mn upon electrochemical cycling, as suggested by the XANES data.

(30) Upon 15% substitution of manganese with chromium, the interatomic distance between O_{ax} and O_{eq} for the $T_d \leftrightarrow O_h$ conduction is decreased by 0.03 Å, which is much greater than the shrinkage of the $O_{eq}-O_{eq}$ bond (0.01 Å) for the $O_h \leftrightarrow O_h$ migration.